Optical and Quantum Electronics (2023) 55:374
https://doi.org/10.1007/s11082-023-04630-1

Performance analysis of coherent DPSK SIMO laser-based satellite-to-ground communication link over weak-to-strong turbulence channels considering Kolmogorov and non-Kolmogorov spectrum models

Ahmed Elsayed Abouelez[1]

Received: 3 December 2022 / Accepted: 27 January 2023 / Published online: 1 March 2023

Abstract
The performance of satellite-to-ground laser-based communication links is highly affected by atmospheric turbulence. Coherent detection with spatial diversity at the ground station receiver can mitigate the scintillation effects caused by atmospheric turbulence. Traditionally, the scintillation effects are modeled based on the Kolmogorov spectrum model. However, the experiments have indicated that scintillation effects on the laser beam propagation have non-Kolmogorov properties. Our goal in the present work is to analyze the average bit error rate (BER), outage probability (OP), and ergodic capacity of the satellite-to-ground heterodyne optical communication system with receiver spatial diversity. A differential phase-shift keying modulation technique is considered in this work. The propagated laser signal from the satellite to the ground station is assumed to be subjected to Málaga-distributed atmospheric turbulence. The atmospheric turbulence statistics are carried out based on the conventional Kolmogorov spectrum model and the three-layer altitude (TLA) non-Kolmogorov spectrum model. The performance of popular diversity combining techniques, namely, maximum ratio combining (MRC) and equal gain combining (EGC) techniques are analyzed. The statistical models of the MRC technique under the Málaga-distributed atmospheric channel model are obtained in analytical form expressions. The statistical models of the EGC technique under the Málaga-distributed atmospheric channel model are obtained via the fast Fourier transform representation of the characteristic function method. Based on these statistical models, average BER, OP, and ergodic capacity expressions for each type of diversity combining technique are derived. For the communication system under investigation, the performance of MRC and EGC multiple aperture receiver systems are compared to a single aperture receiver with the same total aperture area. These comparisons are carried out under the same conditions in terms of zenith angle and signal-to-noise ratio. The obtained results show that the performance of the optical communication system under investigation with MRC and EGC receivers can be improved by increasing the order of diversity. In addition, it is found that the difference in the performance between Kolmogorov and TLA non-Kolmogorov spectrum models is not significant at low zenith angles, while this difference increases as the zenith angle increases. All numerical results are verified by Monte-Carlo simulations.

Extended author information available on the last page of the article

Keywords Satellite optical communications · Atmospheric turbulence · Málaga distribution · Coherent detection · DPSK modulation

1 Introduction

Satellite communication systems are based on conventional radio frequency (RF) bands. Due to the limitations of using RF bands, especially bandwidth constraints, satellites that support free-space laser communication links become more attractive. Free-space laser communication links enjoy several advantages compared to RF communication links. Amongst these advantages; high data rates, cost-effectiveness, high security, and the free license (Andrews and Phillips 2005). Generally, the main problem of optical satellite communications is the fluctuation of amplitude and phase of the optical signal caused by the propagation through an atmospheric turbulence channel. These fluctuations are produced by the refractive index variation owing to the changes in temperature and pressure in the channel (Ata et al. 2022).

Spatial diversity is one of the most powerful techniques that is used to reduce atmospheric turbulence effects. Moreover, coherent optical receivers with homodyne/heterodyne detection are an attractive technique to reduce the undesirable effects of atmospheric turbulence and enhance the overall system performance (Niu et al. 2010, 2011a, b; Ma et al. 2015; Li et al. 2020; Ata et al. 2022; Kumar and Krishnan 2022). Compared to intensity modulation with direct detection (IM/DD) techniques, coherent optical receiver systems offer excellent rejection of background noise and high power efficiency. The main drawback of these systems lies in the complicated detection mechanism compared to IM/DD systems. There are a variety of phase modulation techniques that are used with coherent optical receiver systems, such as binary phase-shift keying (BPSK), quadrature phase-shift keying (QPSK), and differential phase-shift keying (DPSK). Due to the fluctuation of the characteristics of the atmospheric turbulence, BPSK/QPSK demodulation may have phase estimation errors. On the other hand, the received DPSK signal is demodulated by two successive bit intervals and does not require phase noise estimation. Thus, the coherent DPSK can be considered an attractive alternative to BPSK and QPSK for satellite-to-ground laser communication links along with the receiver's spatial diversity (Niu et al. 2011a; Li et al 2020).

Spatial diversity techniques such as selection combining (SC), maximum ratio combining (MRC), and equal gain combining (EGC) have been studied in the cases of terrestrial and satellite coherent optical communication systems (Niu et al. 2010, 2011a, b; Ma et al. 2015; Li et al. 2020). In these scenarios, different atmospheric turbulence statistical models were considered. These statistical models are selected depending on the atmospheric turbulence conditions (Anbarasi et al. 2017). For instance, the log-normal distribution is used to model weak turbulence while the K distribution is used to describe strong turbulence. Gamma-Gamma (GG) distribution is used to describe a wide range of turbulence conditions from weak to strong. In Niu et al. (2011a) the performance of coherent free-space optical communication systems with SC, MRC, and EGC spatial diversity was examined for K-distributed atmospheric turbulence. In Niu et al. (2011b), BPSK and DPSK modulation techniques with EGC and MRC receivers have been studied over GG atmospheric turbulence channels. In Ma et al. (2015), the performance of BPSK satellite-to-ground coherent optical communications with SC and MRC spatial diversity was studied over GG atmospheric turbulence. In Li et al. (2020), the analysis of DPSK satellite-to-ground

coherent optical communication with SC, MRC, and EGC spatial diversity over GG atmospheric turbulence was investigated.

In recent years, a new generalized statistical distribution that can be used to model a wide range of atmospheric turbulence conditions from weak to strong turbulence was introduced by Jurado-Navas et al. (2011). This model is called Málaga distribution. It was shown that Log-normal, GG, and K distributions are special cases of Málaga distribution. Málaga distribution was used as atmospheric turbulence statistical model to evaluate the performance analysis of terrestrial free-space optical communication systems (Samimi and Uysal 2013; Yasser et al. 2021) and optical satellite communication systems (Liu et al. 2021; Wang et al. 2022a; Abouelez 2022).

Moreover, the atmospheric statistics of the previous studies are based on the conventional Kolmogorov spectrum model (Andrews and Phillips 2005). Although the Kolmogorov spectrum model is generally accepted, several works show that the turbulence in portions of the troposphere and stratosphere deviates from the Kolmogorov model (Rao et al. 2000; Golbraikh and Kopeika 2004; Zilberman et al. 2008a, 2010, b; Sheng et al. 2012; Shan et al. 2019). Based on the experimental results of Golbraikh and Kopeika (2004) and Zilberman et al. (2008a), the authors of Zilberman et al. (2008b, 2010) developed a more accurate three-layer altitude (TLA) non-Kolmogorov spectrum model. In this model, it is assumed that the troposphere and lower stratosphere are divided into three main turbulent layers with a constant spectral index in each. Therefore, it becomes acceptable in the literature to use the TLA non-Kolmogorov spectrum model in the studying of the statistics of the irradiance fluctuation that is affected by weak-to-strong turbulence in optical satellite communications (Yi et al. 2013; Yue et al. 2017; Shan et al. 2019; Wang et al. 2022b). For example, the performance of an optical Gaussian beam propagating through weak turbulence from ground to satellite is studied by Yi et al. (2013) considering the TLA non-Kolmogorov spectrum model and log-normal distribution. In Yue et al. (2017), the BER performance analysis is carried out for pulse position modulation (uplink/downlink) laser satellite-communication system where the properties of atmospheric turbulence are described by the TLA non-Kolmogorov spectrum model while the weak-to-strong turbulence channel is modeled by GG distribution. Based on the TLA non-Kolmogorov model, analytical expressions are developed by Shan et al. (2019) to calculate the total scintillation index for the optical Gaussian-beam propagating through (uplink/downlink) satellite communication system taking into consideration the effect of the turbulence outer scale in the stratosphere layer. Recently, in Wang et al. (2022b), the combined effect of three-layer atmospheric turbulence on the wander of an optical Gaussian beam in uplink laser-satellite communication is studied using a TLA non-Kolmogorov spectrum model for vertical/slant path.

The performance analysis of coherent DPSK satellite-to-ground laser communication link with receiver spatial diversity over Málaga atmospheric turbulence considering Kolmogorov and TLA non-Kolmogorov spectrum models, to the best of our knowledge, was not explored previously. Thus, in this work, the Málaga distribution is chosen to model the irradiance fluctuations of DPSK-modulated optical signals that are propagated through the turbulent atmosphere from the satellite to the ground station. The ground station coherent receiver system employs spatial diversity (i.e., single-in multiple-out (SIMO) scenario) to mitigate the effects of atmospheric turbulence. The spatial diversity techniques that are considered in this study are MRC and EGC.

The main contributions in this work can be outlined as follows. Based on the approach given by Shan et al. (2019) for the analysis of the TLA non-Kolmogorov spectrum model, we derived simple expressions for the large-scale and small-scale log irradiance variances of

atmospheric turbulence layers in the case of the unbounded plane wave. Furthermore, the average bit error rate (BER), outage probability (OP), and ergodic capacity are analyzed analytically for the case of the coherent MRC technique. Based on an approximate PDF of the summation of independent and identically distributed (i.i.d.) random variables that follow Málaga PDF (Liu et al. 2021), closed-form expressions of the average BER, OP, and ergodic capacity for the case of MRC diversity are derived. Additionally, for the case of EGC, the exact average BER, OP, and ergodic capacity are obtained based on the numerical representation of the characteristic function (CF) method. Finally, the comparisons between Kolmogorov and TLA non-Kolmogorov spectrum models are made under all turbulence conditions for the coherent optical satellite communication system under consideration. Moreover, all analytical and numerical results are verified by the Monte Carlo (MC) simulations.

The rest of the paper is organized as follows: Sect. 2 describes the model of the coherent optical satellite communication system under investigation. Section 3 introduces the Málaga-distributed channel model which depends on the average power of the optical signal for the line-of-sight (LOS) contribution, the amount of the scattering power coupled to the LOS component, wavelength, satellite height, and refractive index structure. The statistics of considered types of spatial diversity combining techniques are derived in Sect. 4. The average BER, OP, and ergodic capacity expressions are derived in Sect. 5. Section 6 is devoted to presenting numerical and simulation results. Finally, Sect. 7 draws important concluding remarks.

2 System model

In this work, a low earth orbit (LEO) satellite-to-ground optical communication system is considered. The transmitted signal is assumed to be modulated by the DPSK modulation technique. At the ground station, it is assumed that there is a multiple-aperture optical coherent detection receiver with N apertures. The receiver apertures are separated with distances greater than the atmospheric coherence length. Thus, the fading statistics for each can be considered i.i.d. In the coherent optical communication systems that use DPSK, coherent detection is implemented by mixing the beams of the received optical signal and the optical local oscillator. Under consideration of a local oscillator with sufficiently high power compared to the optical signal power, the thermal noise and dark current noise are much smaller than the DC local oscillator current. In this case, the shot noise can be assumed the dominant noise source. It is assumed that the beams of the received optical signal and the local oscillator are mixed in perfect spatial coherence on an adequately small photodetector area. Local oscillator power, P_{LO}, is assumed to be equal for all receiver branches. The generated photocurrent from the nth photodetector is given by (Niu et al. 2011b)

$$i_n(t) = i_{dc,n} + i_{ac,n}(t) + n_n(t) \tag{1}$$

where the DC and AC terms are given by, respectively, $i_{dc,n} = \Re\left(P_n + P_{LO}\right)$ and $i_{ac,n}(t) = \Re\sqrt{2P_nP_{LO}}cos\left(\omega_{IF}t + \varphi\right)$. $\Re$ is the photodetector's responsivity.P_n is the received signal power of the nth branch which is given in terms of the aperture area A_n and the instantaneous received turbulence-dependent optical irradiance I_n as $P_n = A_nI_n$. The intermediate angular frequency, ω_{IF} is defined as the difference between the carrier angular frequency, ω_0, and the local oscillator angular frequency ω_{LO}. $\varphi \in \{0, \pi\}$ symbolizes the phase information. $n_n(t)$ represents the shot noise which can be modeled as a zero-mean additive white Gaussian noise process with a variance which is given by $\sigma_{sh}^2 = 2q\Re P_{LO}\Delta f$ where q is the electron charge and Δf is the noise equivalent bandwidth

of the photodetector (Niu et al. 2011b). From Eq. (1), the instantaneous signal-to-noise ratio (SNR) at the nth branch can be written as

$$\mu_n = \frac{2\Re^2(A_n I_n)P_{LO}}{2q\Re P_{LO}\Delta f} = \frac{\Re(A_n I_n)}{q\Delta f} = \langle \mu_n \rangle I_n \tag{2}$$

where the average SNR per branch is given by $\langle \mu_n \rangle = \Re A_n / q\Delta f$. As will be shown in the numerical and simulation results section, for any number of receiver apertures N, it is assumed that the total area, A_T, of receiver apertures is equal. In other words,A_n in Eq. (2) is equal to A_T/N, $n = 1, \ldots, N$. This assumption is usually used to make a fair comparison between the performance of a single aperture receiver system (i.e., single-in single-out (SISO) communication system) and the performance of a multiple aperture receiver system. Based on this assumption, the total average SNR ratio, for any number of receiver apertures, is given as $\langle \mu_0 \rangle = \Re A_T / q\Delta f$.

There are two diversity combining techniques, which are usually used to combat the influence of atmospheric turbulence, will be considered in this work. The first one is the coherent MRC technique. In this technique, the received signal irradiance for each branch is required to be estimated and the outputs from all branches are weighted properly to maximize combiner SNR. As stated previously, where all branches have photodetector with the same area and responsivity and the atmospheric turbulence of all channels are i.i.d. based on these assumptions, the SNR at the output of the coherent MRC is

$$\mu_{MRC} = \langle \mu_n \rangle \sum_{n=1}^{N} I_n = \langle \mu_n \rangle Z_{MRC} \tag{3}$$

where $Z_{MRC} \triangleq \sum_{n=1}^{N} I_n$. As indicated in Eq. (3), it is required to find the PDF of the sum of i.i.d. Málaga random variables. This PDF and its corresponding CDF will be obtained in Sect. 4.

The second technique of diversity combining that will be addressed in this work is the coherent EGC technique. In this technique, the output SNR from the combiner is the sum of received signal power from each aperture divided by the sum of the noise variances of each aperture (Niu et al. 2011b). Thus, the SNR at the output of the coherent EGC is

$$\mu_{EGC} = \frac{\langle \mu_n \rangle \left(\sum_{n=1}^{N} \sqrt{I_n} \right)^2}{N} = \left(\langle \mu_n \rangle / N \right) Z_{EGC}^2 \tag{4}$$

where $Z_{EGC} \triangleq \sum_{n=1}^{N} \sqrt{I_n}$. As indicated in Eq. (4), it is required to find the PDF of the sum of the square root of i.i.d. Málaga random variables. This PDF and its corresponding CDF are derived in Sect. 4.

3 Channel model

3.1 Scintillation index of a plane wave (Kolmogorov spectrum model)

In the case of a downlink path from a satellite, the diverged beam that is received on the ground can be modeled by a plane wave. Based on extended Rytov theory, the scintillation index, σ_I^2, is given as a function of the large-scale log irradiance variance, σ_{lnX}^2, and small-scale log irradiance variance, σ_{lnY}^2, as (Andrews and Phillips 2005)

$$\sigma_I^2 = exp\left(\sigma_{lnX}^2 + \sigma_{lnY}^2\right) - 1 \tag{5}$$

For the case in which both inner scale and outer scale effects can be ignored and the Kolmogorov power spectrum model (i.e., the power spectrum function $\Phi_n(K) \propto K^{-\alpha}$, where K is the spatial wave number and the spectral exponent value $\tilde{\alpha} = 11/3$ is constant over the slant path) the large-scale and small-scale log irradiance variances are given, respectively, by (Andrews and Phillips 2005).

$$\sigma_{lnX}^2 = \frac{0.49\sigma_R^2}{\left(1 + 1.11\sigma_R^{12/5}\right)^{7/6}} \tag{6a}$$

$$\sigma_{lnY}^2 = \frac{0.51\sigma_R^2}{\left(1 + 0.69\sigma_R^{12/5}\right)^{5/6}} \tag{6b}$$

where the Rytov variance parameter, σ_R^2, for the downlink is given by (Andrews and Phillips 2005)

$$\sigma_R^2 = 2.252k^{7/6}sec^{11/6}(\zeta)\int_{h_0}^{H} C_n^2(h)\left(h - h_0\right)^{5/6}dh \tag{7}$$

In Eq. (7), $k = 2\pi/\lambda$ is the wavenumber, λ is the laser wavelength, ζ is the zenith angle, and h is the satellite altitude. Following the Hufnagle–Vally model that characterizes the variation in turbulence strength, the refractive index structure parameter, $C_n^2(h)$, as a function of altitude h is given by (Andrews and Phillips 2005)

$$C_n^2(h) = 0.00594\left(\frac{u}{27}\right)^2\left(10^{-5}h\right)^{10}exp\left(-\frac{h}{1000}\right) + 2.7\times 10^{-16}exp\left(-\frac{h}{1500}\right) + A_o exp\left(-\frac{h}{100}\right) \tag{8}$$

where u is the wind velocity and A_o is the refractive index structure parameter at the ground.

3.2 Scintillation index of a plane wave (TLA non-Kolmogorov spectrum model)

In the present study, we follow the TLA non-Kolmogorov power spectrum model proposed by Zilberman et al. (2010). Based on experimental results, the authors Zilberman et al. (2010) suggested that the troposphere and lower stratosphere are composed of three main turbulent layers where the spectral exponent value is a constant inside each. The first layer is the boundary layer with Kolmogorov turbulence where the spectrum exponent value is $\tilde{\alpha}_1 = 11/3$. The second layer corresponds to the troposphere with non-Kolmogorov turbulence where the spectrum exponent value is $\tilde{\alpha}_2 = 10/3$. In the third layer, the spectrum exponent value is equal to $\tilde{\alpha}_3 = 5$ in the stratosphere region. Based on this approach, the scintillation index can be given by the following equation (Shan et al. 2019)

$$\sigma_I^2 = exp\left(\sum_{i=1}^{3}\sigma_{lnX\_i}^2 + \sum_{i=1}^{3}\sigma_{lnY\_i}^2\right) - 1 \tag{9}$$

In the above equation, $\sigma^2_{lnX\_i}$ and $\sigma^2_{lnY\_i}$ are the large-scale and small-scale log irradiance variances for *i*th atmospheric turbulence layer. This means that $\sigma^2_{lnX} = \sum_{i=1}^{3} \sigma^2_{lnX\_i}$ and $\sigma^2_{lnY} = \sum_{i}^{3} \sigma^2_{lnY\_i}$.

Based on the TLA non-Kolmogorov model, the authors Shan et al. (2019) developed analytical expressions to calculate the total scintillation index assuming the Gaussian beam taking into consideration the effect of the turbulence outer scale in the stratosphere layer. Based on the approach given in their work, we derived the following simple expressions for the large-scale and small-scale log irradiance variances of *i*th atmospheric turbulence layer in the case of the unbounded plane wave as follows; For the first and second atmospheric layers the large-scale log irradiance variances are given, respectively, by

$$\sigma^2_{lnX_1} = \frac{0.49\sigma^2_{R\_1}}{\left(1 + F_{X\_1}\sigma^{12/5}_{R\_1}\right)^{7/6}} \tag{10a}$$

$$\sigma^2_{lnX_2} = \frac{0.49\sigma^2_{R\_i}}{\left(1 + F_{X\_2}\sigma^{3}_{R\_2}\right)^{4/3}} \tag{10b}$$

where $F_{X_1} = 2.0284\left(\frac{\mu_{1b}}{\mu_{2b}}\right)^{6/7}\left(\frac{\mu_{0b}}{\mu_{1b}}\right)^{6/5}$, $F_{X_2} = 1.011\left(\frac{\mu_{1f}}{\mu_{2f}}\right)^{3/4}\left(\frac{\mu_{0f}}{\mu_{1f}}\right)^{3/2}$. $\sigma^2_{R\_1}$ and $\sigma^2_{R\_2}$ are the scintillation indexes induced by the turbulence in the boundary layer and free troposphere layer, respectively. Their values can be calculated by the following expressions.

$$\sigma^2_{R\_1} = 2.252k^{\frac{7}{6}}sec^{\frac{11}{6}}(\zeta)\left(H - h_0\right)^{\frac{5}{6}}\mu_{1b} \tag{11a}$$

$$\sigma^2_{R\_2} = 2.6176k^{\frac{7}{6}}sec^{\frac{11}{6}}(\zeta)\left(H - h_0\right)^{\frac{5}{6}}\mu_{1f} \tag{11b}$$

The parameters μ_{0b}, μ_{1b}, and μ_{2b} are given, respectively, by $\mu_{0b} = \int_{h_0}^{h_1} C_n^2(h)dh$, $\mu_{1b} = \int_{h_0}^{h_1} C_n^2(h)\xi^{\frac{5}{6}}dh$, and $\mu_{2b} = \int_{h_0}^{h_1} \frac{C_n^2(h)\xi^{-1/3}}{(1-5\xi/8)^{7/5}}dh$. The parameters μ_{0f}, μ_{1f}, and μ_{2f} are given, respectively, by $\mu_{0f} = \int_{h_1}^{h_2} C_n^2(h)dh$, $\mu_{1f} = \int_{h_1}^{h_2} C_n^2(h)\xi^{\frac{2}{3}}dh$, and $\mu_{2f} = \int_{h_1}^{h_2} \frac{C_n^2(h)\xi^{-2/3}}{(1-4\xi/7)^2}dh$. For the downlink path $\xi = \frac{h-h_0}{H-h_0}$. In the third layer, the stratosphere layer, the large-scale log irradiance variance is given by

$$\sigma^2_{lnX_3} \cong (0.53033)\left(\frac{\mu_s}{\mu_{1s}}\right)\sigma^2_{R\_3}\left(\eta^{1/2}_{X\_3} - \eta^{1/2}_{X0\_3}\right) \tag{12a}$$

$$\eta_{X\_3} \approx \frac{(0.853689)\left(\frac{\mu_{1s}}{\mu_s}\right)^2}{1 + F_{X\_3}\sigma^2_{R\_3}} \tag{12b}$$

$$F_{X_3} = \left(\frac{0.170289}{\kappa_0 (k/L)^{-1/2}}\right)\left(\frac{\mu_{1s}}{\mu_{2s}}\right)^2\left(\frac{\mu_{0s}}{\mu_{1s}}\right), \tag{12c}$$

$$\sigma_{R\_3}^2 = 2.177 k^{\frac{7}{6}} sec^{\frac{11}{6}}(\zeta)\left(H - h_0\right)^{\frac{5}{6}} \mu_{1s} \tag{12d}$$

In the above expressions, $\eta_{X\_3} = \frac{\eta_{X\_3} Q_0}{1+\eta_{X\_3} Q_0}$ and $Q_0 = \frac{64\pi^2 L}{k L_0^2}$ where $\kappa_0 = 2\pi/L_0$ and L_0 is the outer scale of the stratospheric turbulence. The parametersμ_{0s},μ_{1s},μ_{2s}, and μ_s are given, respectively, by $\mu_{0s} = \int_{h_2}^{H} C_n^2(h) dh$,$\mu_{1s} = \int_{h_2}^{H} C_n^2(h)\xi^{\frac{3}{2}} dh$, $\mu_{2s} = \int_{h_2}^{H} \frac{C_n^2(h)\xi}{(1-2\xi/3)^{1/2}} dh$, and $\mu_s = \int_{h_2}^{H} C_n^2(h)\xi^2 dh$. Since the outer scale effect is ignored in the Kolmogorov spectrum model described in Sect. 3.1 (i.e. $L_0 \to \infty$), it will be assumed, for comparison between Kolmogorov and TLA non-Kolmogorov spectrum models, that the outer scale of the turbulent has a large value of L_0=200 m (Shan et al. 2019) to satisfy the condition $\lambda L \ll L_0$. The small-scale log irradiance variances of the three layers are given by

$$\sigma_{lnY_{i=1,2,3}}^2 = \frac{0.51\sigma_{R\_i}^2}{\left(1 + F_{Y\_i}\left(\tilde{\alpha}_i\right)\sigma_{R\_i}^{4/(\alpha_i - 2)}\right)^{3-\alpha_i/2}} \tag{13}$$

where $F_{Y_{i=1,2,3}}\left(\tilde{\alpha}_i\right) = [0.4530]^{\frac{2}{2-\alpha_i}}$.

3.3 Atmospheric turbulence model

In the present study, the satellite-to-ground fading channel is modeled by Málaga distribution. This distribution unifies several distributions under certain conditions such as log-normal distribution, GG distribution, and k distribution. Thus, it can be used to model weak to strong atmospheric turbulence. The PDF of the random variable of the received irradiance of the nth path, I_n, which follows the Málaga distribution is given by the formula (Jurado-Navas et al. 2011)

$$f_{I_n}(I) = A\sum_{k=1}^{\beta} a_k I^{\left(\frac{\alpha+k}{2}\right)-1} K_{\alpha-k}\left(2\sqrt{BI}\right), \tag{14a}$$

$$A = \frac{2\alpha^{\frac{\alpha}{2}}}{\gamma^{\frac{\alpha}{2}+1}\Gamma(\alpha)}\left(\frac{\gamma\beta}{\gamma\beta + \overline{\Omega}}\right)^{\beta+\frac{\alpha}{2}}, B = \frac{\alpha\beta}{\gamma\beta + \overline{\Omega}} \tag{14b}$$

$$a_k = \binom{\beta - 1}{k - 1}\frac{\left(\gamma\beta + \overline{\Omega}\right)^{1-\frac{k}{2}}}{(k-1)!}\left(\frac{\overline{\Omega}}{\gamma}\right)^{k-1}\left(\frac{\alpha}{\beta}\right)^{\frac{k}{2}}, \tag{14c}$$

$$\overline{\Omega} = \Omega + 2b_0\rho + 2\sqrt{2b_0\Omega\rho}cos\left(\varphi_A - \varphi_B\right), \tag{14d}$$

$$\gamma = 2b_0(1 - \rho) \tag{14e}$$

In the above equation, $K_v(.)$ is the modified Bessel function of the second kind and order v. $\Gamma(.)$ is the gamma function. α is a positive parameter related to the effective number of large-scale cells of the scattering process and β is a natural number parameter that corresponds to the amount of fading. The average power of the optical signal for the LOS component is denoted by Ω while $2b_0$ denotes the average power of the total scatter component. The parameter $0 \leq \rho \leq 1$ defines the amount of the scattering power coupled to the LOS component. Furthermore, φ_A and φ_B are deterministic phases for the LOS component and the coupled-to-LOS scatter component, respectively. The PDF given by Eq. (6) is normalized such that $I_n = \Omega + 2b_0 = 1$. Following (Andrews & Phillips 2005, Eq. (9-8) and Eq. (9-11)), the fading parameter, α, can be given in terms of large-scale log irradiance variance, σ^2_{lnX}, as follows

$$\alpha = \frac{1}{exp\left(\sigma^2_{lnX}\right) - 1} \tag{15}$$

Moreover, the remaining Málaga distribution parameters (i.e., Ω, ρ, β) can be related to small-scale log irradiance variance, σ^2_{lnY}, by the following equality (Abouelez 2022)

$$exp\left(\sigma^2_{lnY}\right) = \frac{1}{\gamma}\left(\frac{\gamma\beta}{\gamma\beta + \overline{\Omega}}\right)^{\beta} \sum_{r=0}^{\beta-1} \binom{\beta - 1}{r} \times \frac{1}{r}\left(\frac{\overline{\Omega}}{\gamma\left(\gamma\beta + \overline{\Omega}\right)}\right)^{r} \frac{\Gamma(r+3)}{\left(\frac{\beta}{\gamma\beta+\overline{\Omega}}\right)^{r+3}} \tag{16}$$

The right-hand side of Eq. (8) represents the second moment of shadowed-Rician distribution (Jurado-Navas et al. 2011). Equation (16) can be solved, for example, by fixing certain values of Ω and ρ and searching for the nearest value of β that satisfies the equality.

In the case of the Kolmogorov power spectrum model, the large-scale, σ^2_{lnX}, and small-scale, σ^2_{lnX}, log irradiance variances are defined by Eqs. (6a) and (6b), respectively. On the other hand, in the case of the TLA non-Kolmogorov power spectrum model, the large-scale log irradiance variance will be defined as $\sigma^2_{lnX} = \sum_{i=1}^{3} \sigma^2_{lnX\_i}$ and the small-scale log irradiance variance will be defined as $\sigma^2_{lnY} = \sum_{i}^{3} \sigma^2_{lnY\_i}$ where $\sigma^2_{lnX\_i}$ and $\sigma^2_{lnY\_i}$ are the large-scale and small-scale log irradiance variances for ith atmospheric turbulence layer. $\sigma^2_{lnX\_i}$ values can be calculated by Eqs. (10a), (10b), and (11a) while $\sigma^2_{lnY\_i}$ values can be calculated by Eq. (13).

Finally, the CDF of the Málaga distribution is given by the following equation

$$F_{I_n}\left(I_t\right) = \int_0^{I_t} f_{I_n}(I)dI = A\sum_{k=1}^{\beta} a_k \left[\int_0^{I_t} I^{\left(\frac{\alpha+k}{2}\right)-1} K_{\alpha-k}\left(2\sqrt{BI}\right)dI\right] \tag{17}$$

The integration inside the bracket can be given in closed form as follows: First, the modified Bessel function of the second kind. $K_v(x)$, is represented in terms of Meijer's G function with help of Eq. (9.34.3) from Gradshteyn and Ryzhik (2014).

$$\int_0^{I_t} I^{\left(\frac{\alpha+k}{2}-1\right)} K_{\alpha-k}\left(2\sqrt{BI}\right)dI = \frac{1}{2}\int_0^{I_t} I^{\left(\frac{\alpha+k}{2}-1\right)} G^{2,0}_{0,2}\left(BI\middle|\begin{matrix} - \\ \frac{\alpha-k}{2}, \frac{k-\alpha}{2}\end{matrix}\right)dI \tag{18}$$

Second, with help of Eq. (7.811.2) from Gradshteyn and Ryzhik (2014) which has the following form $\int_0^1 x^{(\delta-1)} G^{m,n}_{p,q}\left(\vartheta x\middle|\begin{matrix}\mathrm{a}\\ \mathrm{b}\end{matrix}\right)dx = G^{m,n+1}_{p+1,q+1}\left(\vartheta\middle|\begin{matrix}1-\delta, \mathrm{a}\\ \mathrm{b}, -\delta\end{matrix}\right)$ and letting $x = I/I_t$, and

identifying $\delta = \left(\frac{\alpha+k}{2}\right)$ and $\vartheta = 2\sqrt{BI_t}$, then substituting in Eq. (18) we will have a closed-form expression for the Málaga distribution CDF function as follows

$$F_{I_n}(I_t) = \frac{A}{2} I_t^{\frac{\alpha}{2}} \sum_{k=1}^{\beta} a_k I_t^{\frac{k}{2}} G_{1,3}^{2,1}\left(BI_t \middle| \begin{matrix} 1-\kappa_1;- \\ \kappa_2, \kappa_3; -\kappa_1 \end{matrix} \right) \tag{19}$$

where $\kappa_1 = (\alpha + k)/2$, $\kappa_2 = (\alpha - k)/2$, and $\kappa_3 = (k - \alpha)/2$.

In the following section, the statistics corresponding to each type of diversity combining receiver are illustrated. These statistics correspond to the summation of random variables related to the Málaga distribution.

4 Statistics of diversity combining techniques

4.1 MRC receiver statistics

As it is mentioned in Sect. 2, the performance analysis of MRC depends on finding a PDF of the summation of i.i.d. random variables $I_n, n = 1, \ldots, N$ that follow Málaga PDF. If a sum of multiple Málaga random variables is defined as $Z_{MRC} \triangleq \sum_{n=1}^{N} I_n$, an approximate PDF to Z_{MRC} can be given by the following equation (Liu et al. 2021)

$$f_{Z_{MRC}}(Z_{MRC}) = A_N \sum_{k=0}^{N(\beta-1)} a_{N,k} Z_{MRC}^{\left(\frac{N\alpha+N+k}{2}-1\right)} \times K_{N\alpha-N-k}\left(2\sqrt{NBZ_{MRC}}\right) \tag{20a}$$

$$a_{N,k} = \begin{pmatrix} N\beta - 1 \\ N(\beta-1) - k \end{pmatrix} \frac{1}{k!} \left(\frac{\overline{\Omega}}{\gamma\left(\gamma\beta + \overline{\Omega}\right)} \right)^k \times \left(\frac{\beta}{\left(\gamma\beta + \overline{\Omega}\right) N\alpha} \right)^{\frac{N\alpha-N-k}{2}} \tag{20b}$$

$$A_N = \frac{2\Gamma(N\beta - N + 1)(N\alpha)^{N\alpha}}{\gamma^N \Gamma(N\beta)\Gamma(N\alpha)} \left(\frac{\gamma\beta}{\gamma\beta + \overline{\Omega}} \right)^{N\beta} \tag{20c}$$

The CDF of the random variable Z_{MRC} is given by the following equation

$$F_{Z_{MRC}}(I_t) = \int_0^{I_t} f_{Z_{MRC}}(Z_{MRC}) dZ_{MRC} = A_N \sum_{k=0}^{N(\beta-1)} a_{N,k} \times \left[\int_0^{I_t} Z_{MRC}^{\left(\frac{N\alpha+N+k}{2}-1\right)} K_{N\alpha-N-k}\left(2\sqrt{NBZ_{MRC}}\right) dZ_{MRC} \right] \tag{21}$$

Following the same steps used to find Eq. (19), the CDF given by Eq. (21) can be given in the following form

$$F_{Z_{MRC}}(I_t) = \frac{A_N}{2} I_t^{\frac{N(\alpha+1)}{2}} \sum_{k=0}^{N(\beta-1)} a_{N,k} I_t^{\frac{k}{2}} G_{1,3}^{2,1}\left(NBI_t \middle| \begin{matrix} 1-\kappa_4;- \\ \kappa_5, \kappa_6; -\kappa_4 \end{matrix} \right) \tag{22}$$

where $\kappa_4 = (N\alpha + N + k)/2$, $\kappa_5 = (N\alpha - N - k)/2$, and $\kappa_6 = (N + k - N\alpha)/2$.

4.2 EGC receiver statistics

The performance analysis of EGC depends on finding the PDF of the random variable $Z_{EGC} = \sum_{n=1}^{N} \sqrt{I_n}$ where the random variable $I_n, n = 1, \ldots, N$ follows Málaga PDF.

It is very difficult to obtain the PDF of Z_{EGC} in a closed form. This difficulty is due to the Málaga random variable I_n is derived from a product of two independent random variables, i.e., $I_n = X_n Y_n$ (Jurado-Navas et al. 2011), in which X_n follows the Gamma distribution while Y_n is related to the Shadowed–Rician distribution (i.e., Y_n is calculated by squaring the absolute value of the Shadowed–Rician random variable). Thus, to derive the PDF of the random variable $Z_{EGC} = \sum_{n=1}^{N} \sqrt{I_n}$ we need first to find the PDF and the moment generating function (MGF) of the sum of Nakagami-*m* random variables and the PDF and MGF of the sum of Shadowed–Rician random variables. From the literature review, the PDF and the MGF of the sum of Nakagami-*m* random variables have very complex expressions (Dharmawansa et al. 2007) while the derivation of PDF and MGF of the sum of Shadowed-Rician random variables, to the best of our knowledge, is an open point of research.

In the present work, the PDF of Z_{EGC} will be obtained numerically as follows: Denoting the square root of the random variable I_n as z_n (i.e., $z_n = \sqrt{I_n}$), the PDF of z_n is obtained from the PDF given by Eq. (14a) by using random variable transformation as

$$f_{z_n}(z_n) = 2A \sum_{k=1}^{\beta} a_k z_n^{(\alpha+k)-1} K_{\alpha-k}\left(2\sqrt{B} z_n\right) \tag{23}$$

From the basic definition of the CF of the PDF (Osche 2002), the CF can be computed numerically by using the fast Fourier transform (FFT). Since the random variables $z_n \triangleq \sqrt{I_n}$ are i.i.d., so the CF of the random variable Z_{EGC} can be defined as $G_{Z_{EGC}}(iv) \triangleq \left[FFT\left(f_{z_n}(z_n)\right)\right]^N$. Thus, the PDF of Z_{EGC} can be defined as $f_{Z_{EGC}}(Z_{EGC}) \triangleq IFFT\left[G_{Z_{EGC}}(iv)\right]$ where IFFT denotes the inverse FFT. The numerical calculations can be outlined as follows: First, the PDF given by Eq. (23) is discretized with equal steps Δz. The number of discretization steps, s, and Δz are chosen to satisfy the condition $\int_0^\infty f_{z_n}(z_n) dz \cong 1$. This integration is implemented numerically. Second, the FFT of discretized $f_{z_n}(z_n)$ is calculated. Then, the CF of the random variable Z_{EGC} is calculated according to the numerical definition $G_{Z_{EGC}}(iv) \triangleq \left[FFT\left(f_{z_n}(z_n)\right)\right]^N$. The obtained CF, $G_{Z_{EGC}}(iv)$, has a total number of discretization steps equal to $(sN - 1)$. Finally, the PDF of the random variable Z_{EGC} can be obtained easily by computing the IFFT of $G_{Z_{EGC}}(iv)$ according to the following equation

$$f_{Z_{EGC}}(Z_{EGC}) = (\Delta z)^{N-1} IFFT\left[G_{Z_{EGC}}(iv)\right] \tag{24}$$

It is important to express that the FFT and IFFT calculation steps can be easily implemented by using numerical convolution. By using this method, discretized $f_{z_n}(z_n)$ is convolved $(N - 1)$ times with itself. The CDF of the random variable Z_{EGC} can be calculated numerically by using the standard definition of CDF as follow

$$F_{Z_{EGC}}(Z_{th}) = \int_0^{Z_{th}} f_{Z_{EGC}}(Z_{EGC}) dZ_{EGC} \tag{25}$$

5 Performance analysis

In this section, the performance of the coherent communication system under consideration will be studied in terms of the average BER, the OP, and the ergodic capacity. The conditional BER equation for a communication system using DPSK is given by (Proakis 2001)

$$P_{e,DPSK}(Z) = \frac{1}{2} exp\left(-\mu_Z\right) \tag{26}$$

where μ_Z is the instantaneous average SNR given by Eqs. (3) and (4) in the case of MRC and EGC, respectively. The average BER is defined as

$$BER = \int_0^\infty P_{e,DPSK}(Z) f_Z(Z) dZ \tag{27}$$

where $f_Z(Z)$ is the PDF corresponding to the random variable Z related to the Málaga distribution. In addition, the OP is defined as the probability of the instantaneous SNR, μ, being less than a predefined threshold. In other words, the OP can be found by calculating the CDF of the instantaneous SNR. This definition can be expressed as follows

$$P_{out} = \Pr\left(\mu < \mu_{th}\right) = \int_0^{\mu_{th}} f_\mu(\mu) d\mu \tag{28}$$

The maximum data rate that can be provided through the communication channel is called the channel capacity. The normalized form of the instantaneous channel capacity is given by $C = log_2\left(\mu_Z + 1\right)$. The channel capacity, C, is a random variable, and its average value, C, (i.e., ergodic capacity) can be defined as

$$C = \int_0^\infty log_2\left(\mu_Z + 1\right) f_Z(Z) dZ \tag{29}$$

In the following subsections, the equations of the average BER and OP are obtained for each case of diversity combining techniques.

5.1 MRC receiver

The average BER of DPSK under a coherent MRC receiver is given by substituting Eqs. (20) and (26) in Eq. (27) as follows

$$BER_{MRC} = \frac{A}{2} \sum_{k=0}^{N(\beta-1)} a_k \int_0^\infty Z_{MRC}^{\kappa_4 - 1} exp\left(-\langle \mu_n \rangle Z_{MRC}\right) \times K_{N\alpha - N - k}\left(2\sqrt{NBZ_{MRC}}\right) dZ_{MRC} \tag{30}$$

By making the change of variable, $Z_{MRC} = x^2$ then $dz/dx = 2x$, we will have

$$BER_{MRC} = \sum_{k=0}^{N(\beta-1)} Aa_k \left[\int_0^{\infty} x^{(N\alpha+N+k-1)} exp\left(-\mu_0 x^2\right) \times K_{N\alpha-N-k}\left(2\sqrt{NB}x\right) dx \right] \tag{31}$$

The integration inside the brackets can be solved with the help of Eq. (6.631.3) from Gradshteyn and Ryzhik (2014). Thus, the average BER in the case of MRC can be expressed as follows

$$BER_{MRC} = \sum_{k=0}^{N(\beta-1)} \left(\frac{A\Gamma(N\alpha)}{4\sqrt{NB}} exp\left(\frac{NB}{2\langle\mu_n\rangle}\right) \right) \times \left[a_k \overline{\mu}^{\frac{-\mu_k}{2}} \Gamma(N+k) W_{\frac{-\mu_k}{2},\frac{\nu_k}{2}}\left(\frac{NB}{\langle\mu_n\rangle}\right) \right] \tag{32}$$

where $W_{\frac{-\mu}{2},\frac{\nu}{2}}(z)$ is Whittaker W function (Abramowitz and Stegun 1970), $\mu_k = (N\alpha + N + k - 1)$ and $\nu_k = (N\alpha - N - k)$. Although Eq. (31) is a closed-form expression for the BER_{MRC}, it is best, from a computational point of view, to calculate the BER_{MRC} by Eq. (30) through numerical integration.

From Eqs. (3) and (28), the OP of the MRC receiver can be defined as $Pr\left(Z_{MRC} < \frac{\mu_{th}}{\mu_0}\right)$ which can be obtained directly from Eq. (22) as follows

$$P_{out}^{MRC} = \frac{A_N}{2} \left(\frac{\mu_{th}}{\langle\mu_n\rangle}\right)^{\frac{N(\alpha+1)}{2}} \sum_{k=0}^{N(\beta-1)} a_{N,k} \left(\frac{\mu_{th}}{\langle\mu_n\rangle}\right)^{\frac{k}{2}} \times G_{1,3}^{2,1}\left(NB\left(\frac{\mu_{th}}{\langle\mu_n\rangle}\right) \middle| \begin{matrix} 1-\kappa_4; - \\ \kappa_5, \kappa_6; -\kappa_4 \end{matrix} \right) \tag{33}$$

From Eqs. (3) and (29), the ergodic capacity of the MRC receiver can be given as follows

$$\boldsymbol{C_{MRC}} = \boldsymbol{A_N} \sum_{k=0}^{N(\beta-1)} \boldsymbol{a_{N,k}} \int_0^{\infty} \boldsymbol{log_2}\left(\boldsymbol{\mu_n Z_{MRC}} + 1\right) \boldsymbol{Z_{MRC}^{(\kappa_4-1)}} \boldsymbol{K_{N\alpha-N-k}}\left(2\sqrt{\boldsymbol{NBZ_{MRC}}}\right) \boldsymbol{dZ_{MRC}} \tag{34}$$

The Bessel function and logarithmic function can be expressed in their equivalent Meijer's G functions with the help of Eq. (9.34.3) from Gradshteyn and Ryzhik (2014), and Eq. (07.34.03.0456.01) from (https://functions.wolfram.com/), respectively. Thus, Eq. (34) can be written in the following form

$$\boldsymbol{C_{MRC}} = \frac{\boldsymbol{A_N}}{2\boldsymbol{ln2}} \sum_{k=0}^{N(\beta-1)} \boldsymbol{a_{N,k}} \left[\int_0^{\infty} \boldsymbol{Z_{MRC}^{(\kappa_4-1)}} \boldsymbol{G_{2,2}^{1,2}}\left(\boldsymbol{\mu_n Z_{MRC}} \middle| \begin{matrix} 1,1 \\ 1,0 \end{matrix} \right) \boldsymbol{G_{0,2}^{2,0}}\left(\boldsymbol{NBZ_{MRC}} \middle| \begin{matrix} - \\ \boldsymbol{\kappa_5}, \boldsymbol{\kappa_6} \end{matrix} \right) \boldsymbol{dZ_{MRC}} \right] \tag{35}$$

The integral inside the bracket can be evaluated with the help of Eq. (07.34.21.0011.01) from (https://functions.wolfram.com/). Thus, we can obtain the ergodic capacity of the MRC receiver in the following closed form

$$\boldsymbol{C_{MRC}} = \frac{\boldsymbol{A_N}}{2\boldsymbol{ln2}} \sum_{k=0}^{N(\beta-1)} \boldsymbol{a_{N,k}} \boldsymbol{\mu_n^{-\kappa_4}} \boldsymbol{G_{2,4}^{4,1}}\left(\frac{\boldsymbol{NB}}{\boldsymbol{\mu_n}} \middle| \begin{matrix} \{-\boldsymbol{\kappa}_4\};\{1-\boldsymbol{\kappa}_4\} \\ \{\boldsymbol{\kappa_5}, \boldsymbol{\kappa_6}, -\boldsymbol{\kappa}_4, -\boldsymbol{\kappa}_4\};\{-\} \end{matrix} \right) \tag{36}$$

5.2 EGC receiver

The average BER of DPSK under a coherent EGC receiver is given by substituting Eqs. (24) and (26) in Eq. (27) as follows

$$BER_{EGC} = \int_0^{\infty} f_{Z_{EGC}}(Z_{EGC}) exp\left(-\left(\langle \mu_n \rangle / N\right) Z_{EGC}^2\right) dZ_{EGC} \tag{37}$$

From Eqs. (4) and (28), the OP of the EGC receiver can be defined as $Pr\left(Z_{EGC} < \sqrt{\frac{\mu_{th}}{(\langle \mu_n \rangle / N)}}\right)$ obtained which can be obtained directly from Eq. (25) as follows

$$P_{out}^{EGC} = \int_0^{\sqrt{\frac{\mu_{th}}{(\langle \mu_n \rangle / N)}}} f_{Z_{EGC}}(Z_{EGC}) dZ_{EGC} \tag{38}$$

From Eqs. (4) and (29), the ergodic capacity of the EGC receiver can be given as follows

$$C_{EGC} = \int_0^{\infty} log_2\left(\left(\langle \mu_n \rangle / N\right) Z_{EGC}^2 + 1\right) f_{Z_{EGC}}(Z_{EGC}) dZ_{EGC} \tag{39}$$

In the following section, the derived equations of the average BER, the OP, and the ergodic capacity for each diversity combining technique will be used to investigate the performance of each one under satellite-to-ground laser communication links over the Málaga turbulence channel.

6 Results and discussion

In this section, the average BER, OP, and ergodic capacity of coherent DPSK LEO satellite-to-ground laser communication system over the Málaga fading channel are presented. The results are obtained under consideration of the Kolmogorov spectrum model and the TLA non-Kolmogorov spectrum model. The parameters used for the optical communication system under consideration are presented in Table 1.

Figure 1 plots the scintillation index as a function of the zenith angle in the range (0°–88°) based on the TLA non-Kolmogorov spectrum model [i.e. Eq. (9)] and the Kolmogorov spectrum model [i.e. Eq. (5)]. As can be noted from the figure, the scintillation index due to TLA non-Kolmogorov spectrum model is higher than the scintillation index due Kolmogorov model for a wide range of the zenith angle (0°–84°). The difference in scintillation index values of the two models is very small at low zenith angles (nearly less than 50°) and increases as the zenith angle increases. Moreover, the scintillation index values for the two models increase as the zenith angle increase until they reach their maximum values at zenith angles of (85°) in the case of the TLA non-Kolmogorov model and (86°) in the case of the Kolmogorov model, then their values decrease again.

Since the scintillation index values are zenith-angle dependent, thus, the Málaga PDF parameters (i.e., α, β) values are varying, also, according to the assumed values of the zenith angle, ζ. Based on the obtained results from Fig. 1, we can choose three different

Table 1 Numerical simulation parameters

Parameter	Value
Wavelength, λ	1550 nm
Wind velocity, $\boldsymbol{u}$	21 m/s
Refractive-index structure parameter, $\boldsymbol{A_o}$	1.7×10^{-14} $m^{-2/3}$
Height of the boundary layer, $\boldsymbol{h_1}$	2 km
Height of the free troposphere layer, $\boldsymbol{h_2}$	9 km
The altitude of the satellite, $\boldsymbol{H}$	500 km
Outage probability SNR threshold, $\boldsymbol{\mu_{th}}$	10 dB

values of the zenith angle to examine the performance of the satellite optical communication system under investigation due to the effect of the optical wave propagation from the satellite to the ground station through Kolmogorov and TLA non-Kolmogorov turbulence. These values represent the strength of turbulence and are taken to be equal to 25°, 65°, and 80° for weak, moderate, and strong turbulence, respectively.

To calculate Málaga distribution parameters according to the assumed system parameters in Table 1, we assume, for simplicity, that the average power of the optical signal for the LOS component, Ω, is 0.99, $\varphi_A - \varphi_B = \pi/2$, and ρ is 0.999 overall zenith angle values. Since $\rho \to 1$, the Málaga distribution, in this case, tends to be the GG distribution (Jurado-Navas et al. 2011). Thus, the parameters α and β can be obtained in terms of assumed channel parameters through Eqs. (15) and (16), respectively. Table 2 summarizes the calculated values of α and β for each assumed value of ζ. Moreover, as stated in Sect. 2, it is assumed that the total area of receiver apertures is equal to the aperture area of the single receiver (i.e., SISO scenario). This assumption displays the expected improvement of each spatial diversity technique on the performance of the optical communication system under examination.

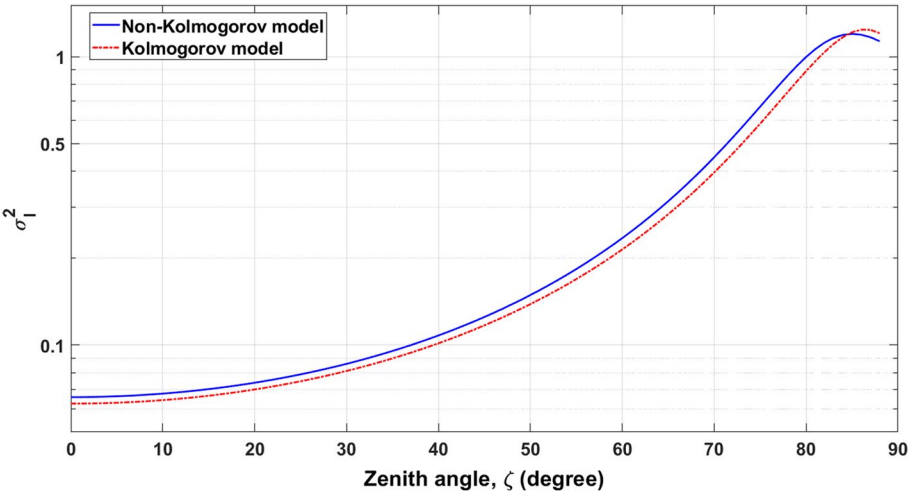

Fig. 1 Scintillation index as a function of the zenith angle for a satellite-to-ground downlink link in the case of the TLA non-Kolmogorov model (solid curve) and conventional Kolmogorov model (dash-dot curve)

Concerning MC simulation, the parameters Ω, ρ, α, and β are used to generate random variables that follow the Málaga distribution. Since the satellite communication systems send and receive data with bitrate in the order of multi Mb/s, the channel characteristics are assumed to remain constant for at least two successive bit intervals. This is an essential condition for the DPSK communication system which needs a constant channel characteristic for at least two successive bit intervals to work properly (Niu et al. 2011b; Kiasaleh 2006). Based on this condition, every two successive bits which are randomly generated are impaired by one Málaga random variable. A sufficient number of random bits are generated to simulate average BER $> 10^{-9}$.

Figure 2 depicts the average BER as a function of the total average SNR in the case of SISO, MRC, and EGC spatial diversity techniques for different values of the zenith angle considering Kolmogorov and TLA non-Kolmogorov spectrum models. Figure 2a shows the average BER performance of a single aperture receiver system ($N = 1$). The average BER performances of the coherent MRC receiver are shown in Fig. 2b, c while the average BER performances of the coherent EGC receiver are shown in Fig. 2d, e. These arrangements are for receiver apertures equal to $N=2$ and 3, respectively. As can be seen, the MC simulation results are in good agreement with the numerical results.

Generally, the average BER performance for all diversity combining techniques decreases as the average SNR increases. Also, it decreases as the zenith angle decreases (i.e., the laser beam turns from a strong turbulent channel to a weak turbulent channel). The average BER performances of MRC and EGC receiver systems outperform the SISO system. It can be noted that as the number of apertures increases the average BER decreases.

Additionally, the results shown in Fig. 2 show that the difference in the average BER performances between Kolmogorov and TLA non-Kolmogorov spectrum models is not significant at low zenith angle (weak turbulence) and decrease as the number of receiver apertures increase for both MRC and EGC receiver systems. As the zenith angle increase (moderate to strong turbulence), the difference becomes more significant, especially in the case of EGC receiver systems. For example, at an average BER of 1×10^{-9} and $\zeta = 80^{\circ}$ it can be observed from Fig. 2c, f (i.e.,$N = 3$) that there is a nearly 1.5 dB average SNR difference between Kolmogorov and TLA non-Kolmogorov spectrum models in the case of MRC while there is nearly 2 dB average SNR difference between Kolmogorov and TLA non-Kolmogorov spectrum model in the case of EGC receivers. Moreover, as expected from previous studies, it can be noted that both MRC and EGC receivers have a comparable performance under the consideration of the Kolmogorov or TLA non-Kolmogorov spectrum model. For example, at an average BER of 1×10^{-9} and $\zeta = 80^{\circ}$ it can be noted from Fig. 2c, f that there is a nearly 1 dB average SNR difference between the MRC and EGC receivers in the case of Kolmogorov and TLA non-Kolmogorov spectrum models.

Figure 3 shows the OP versus the total average SNR in the case of SISO, MRC, and EGC spatial diversity techniques for different values of the zenith angle considering

Table 2 Málaga PDF parameters

ζ	Kolmogorov model		TLA non-Kolmogorov model	
	α	β	α	β
25°	28.1902	26	26.1356	25
65°	8.3298	7	6.7462	7
80°	4.0362	2	2.4117	2

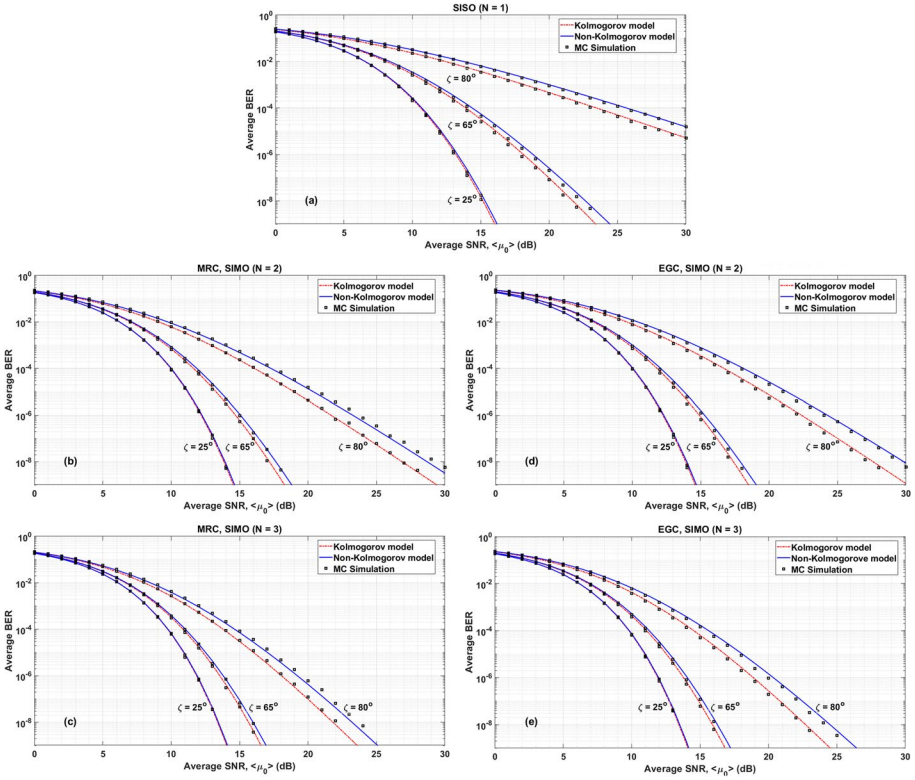

Fig. 2 Average BER of coherent DPSK satellite-to-ground laser link over Málaga atmospheric turbulence and different spatial diversity techniques considering Kolmogorov and TLA non-Kolmogorov spectrum models; **a** for SISO; **b**, **c** for MRC; **d**, **e** for EGC, at different values of zenith angles

Kolmogorov and TLA non-Kolmogorov spectrum models. Figure 3a shows the OP of the single aperture receiver system ($N = 1$). The OP performances of the coherent MRC receiver are shown in Fig. 3b, c while the OP performances of the coherent EGC receiver are shown in Fig. 3d, e. These arrangements are for receiver apertures equal to $N = 2$ and 3, respectively.

The OP for all cases is calculated assuming the OP with an SNR threshold of 10 dB. It can be observed that there is good matching between MC simulation results and numerical results. Since the analytical analysis of the OP, and the ergodic capacity, in the case of the MRC spatial diversity technique depends mainly on the approximate PDF given by Eq. (20), there are some slight deviations, which can be observed, between exact MC simulation results and approximate analytical results at $\zeta = 80^{\circ}$. For more clarification, Eq. (20) is an approximate PDF of the sum of Málaga random variables (Liu et al. 2021) with a certain small error which has a mean value equal to zero and variance that is inversely proportional to the values of α and β and directly proportional to the number of receiver apertures N (Chatzidiamantis and Karagiannidis 2011). So, it is clear that the error variance increases at higher values of the zenith angle, especially at $\zeta = 80^{\circ}$ (corresponding to lower values of α and β) and a higher number of receiver apertures. Thus, a small error can be noted between the approximate analysis of

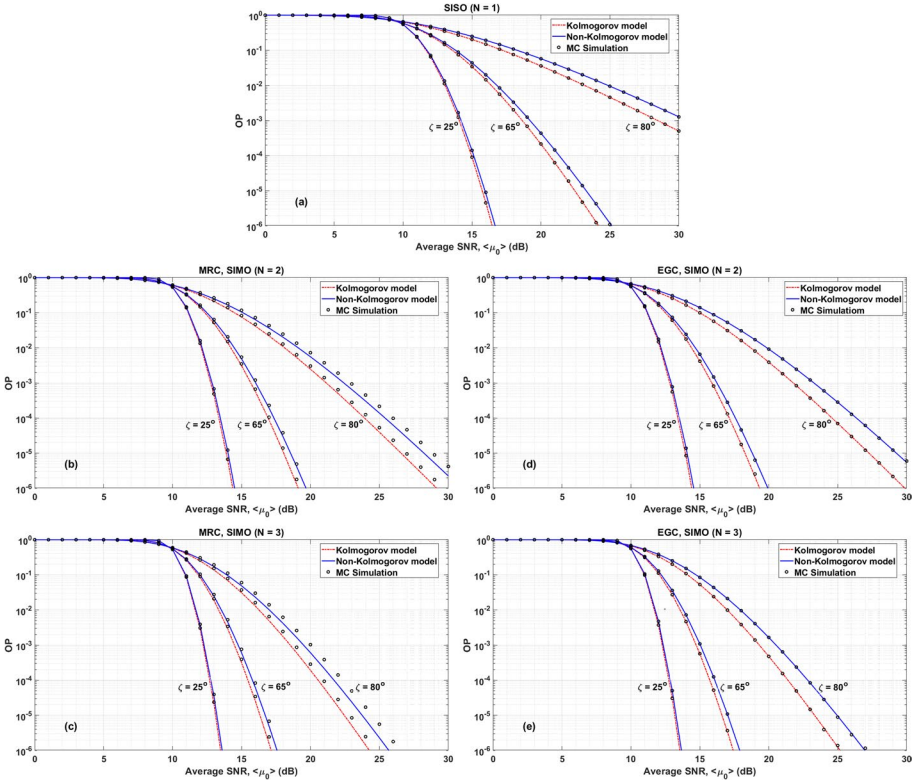

Fig. 3 OP of coherent DPSK satellite-to-ground laser link over Málaga atmospheric turbulence and different spatial diversity techniques considering Kolmogorov and TLA non-Kolmogorov spectrum models; **a** for SISO; **b**, **c** for MRC; **d**, **e** for EGC, at different values of zenith angles

the OP and ergodic capacity, as will be shown, and the exact analysis given by the MC simulation.

Generally, the OP for all diversity combining techniques decreases as the total average SNR becomes greater than the OP SNR threshold. Also, it decreases as the zenith angle decreases as the laser beam turns from a strong turbulent channel to a weak turbulent channel. The OP performances of MRC and EGC receiver systems outperform the SISO system. For all assumed values of the zenith angle, as the number of receiver apertures increases the OP decreases.

The results shown in Fig. 3 indicate that the difference in the OP between Kolmogorov and TLA non-Kolmogorov spectrum models is not, also, significant at low zenith angle (weak turbulence) and decrease as the number of receiver apertures increase for both MRC and EGC receiver systems. As the zenith angle increase (moderate to strong turbulence), the difference becomes more significant, especially in the case of EGC receiver systems. For example, at OP of 1×10^{-6} and $\zeta = 80^{\circ}$ it can be noted from Fig. 3c, f (i.e.,$N = 3$) that there is a nearly 1.5 dB average SNR difference between Kolmogorov and TLA non-Kolmogorov spectrum models in the case of MRC while there is nearly 2 dB average SNR difference between Kolmogorov and TLA non-Kolmogorov spectrum model in the case of EGC receivers. In addition, it can be noted that both

MRC and EGC receivers have comparable OP performance under the consideration of the Kolmogorov and TLA non-Kolmogorov spectrum models. For instance, at OP of 1×10^{-6} and $\zeta = 80^{\circ}$ it can be noted from Fig. 3c, f that there is nearly 1 dB and average SNR difference between the MRC and EGC receivers in the case of Kolmogorov and TLA non-Kolmogorov spectrum models.

Figure 4 shows the ergodic capacity performances as a function of the total average SNR in the case of SISO, MRC, and EGC spatial diversity techniques for different values of the zenith angle considering Kolmogorov and TLA non-Kolmogorov spectrum models. Figure 4a shows the ergodic capacity of a single aperture receiver system ($N = 1$). The ergodic capacity performances of the coherent MRC receiver are shown in Fig. 4b, c while the ergodic capacity performances of the coherent EGC receiver are shown in Fig. 4d, e. These arrangements are for receiver apertures equal to $N = 2$ and 3, respectively.

As illustrated, for all cases (i.e., SISO, MRC, and EGC), the ergodic capacity performances increase as the average SNR increase. In addition, although the ergodic capacity performances under all zenith angles are very close together, there is a slight performance enhancement as the zenith decrease (i.e. the atmospheric turbulence goes from strong to weak). Also, the notable difference in ergodic capacity performances

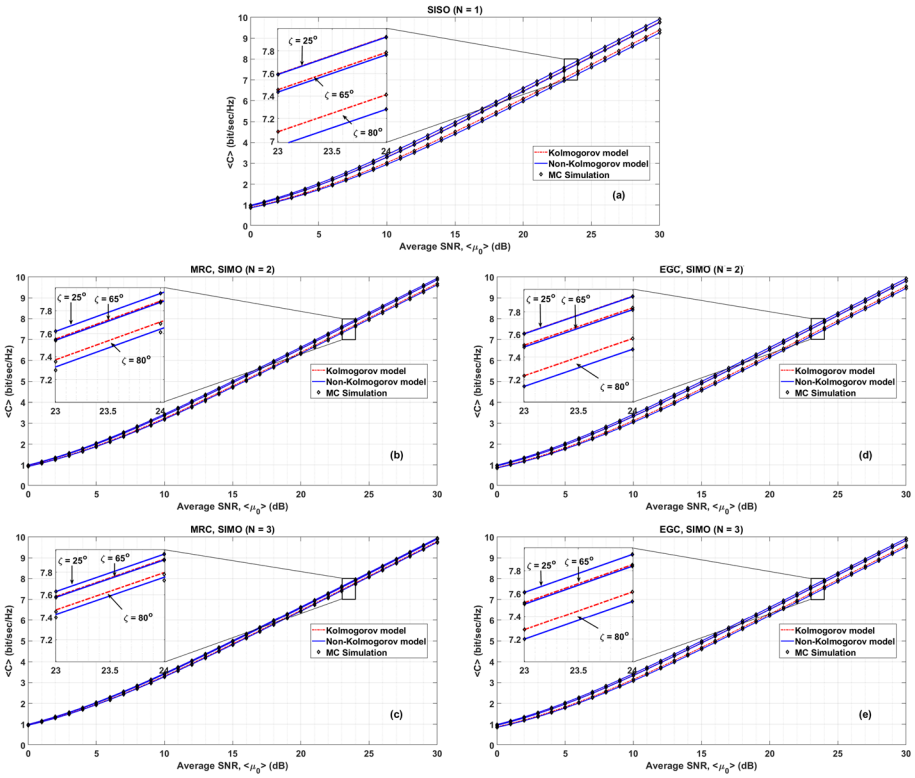

Fig. 4 Ergodic capacity of coherent DPSK satellite-to-ground laser link over Málaga atmospheric turbulence and different spatial diversity techniques considering Kolmogorov and TLA non-Kolmogorov spectrum models; **a** for SISO, **b**, **c** for MRC; **d**, **e** for EGC, at different values of zenith angles

between Kolmogorov and TLA non-Kolmogorov spectrum models is at strong turbulence ($\zeta = 80^{\circ}$). This difference decrease as the number of receiver apertures increases especially in the case of MRC. Moreover, there is a good match between the numerical results and MC simulation results.

From the obtained results, some remarks can be outlined as follows: the comparable performance between EGC and MRC receivers at any number of receiver apertures makes EGC offers a good alternative to MRC with reduced complexity. The average BER, OP, and ergodic capacity performances of coherent detection can be improved by increasing in diversity order for all values of the zenith angle. The difference in the performance, for the optical communication system under consideration, between Kolmogorov and TLA non-Kolmogorov spectrum models is not significant at low zenith angles (weak turbulence), while this difference increases as the zenith angle increases (moderate to strong turbulence). This difference can be slightly reduced by increasing the number of receiver apertures especially by considering the MRC technique.

7 Conclusions

The impact of the Málaga-distributed atmospheric turbulence channel on coherent DPSK LEO satellite-to-ground laser communication link with receiver spatial diversity considering Kolmogorov and TLA non-Kolmogorov spectrum models is investigated. The diversity combining techniques that are considered in this study are MRC and EGC. Firstly, we derived the PDF and CDF equations that model the random fluctuation of the output signal from each type of diversity combining receivers. These equations are used to derive the average BER, the OP, and the ergodic capacity expressions to investigate the performance of the coherent DPSK satellite-to-ground laser communication link over Málaga atmospheric turbulence in the cases of MRC and EGC receivers. The exactness of the derived expressions is verified by MC simulations. The effects of the received SNR, number of receiver apertures, and zenith angle on the system performance are studied considering Kolmogorov and TLA non-Kolmogorov spectrum models. The average BER and the OP of the coherent MRC and EGC receivers were compared to the single aperture receiver system with an aperture area equal to the total aperture areas of any type of diversity combining receivers. The obtained results show that the coherent MRC and EGC receivers outperform the single aperture receiver and the performance of the systems under investigation is highly improved by increasing the number of receiver apertures. In addition, it is noted that the performance of the coherent EGC provides comparable performance to that of the coherent MRC which makes EGC offers a good alternative to MRC with reduced complexity. Additionally, it is found that the difference in the performance, for the optical communication system under consideration, between Kolmogorov and TLA non-Kolmogorov spectrum models is not significant at low zenith angles (weak turbulence), while this difference increases as the zenith angle increases (moderate to strong turbulence). This difference can be slightly reduced by increasing the number of receiver apertures.

Acknowledgements The author would like to thank Prof. Essam A. Eldiwany at Electronics Research Institute for his insightful discussions.

Author contributions All authors contributed to the study's conception and design. The analysis was performed by A.A. The first draft of the manuscript was written by A.A. All authors read and approved the final manuscript.

Funding Open access funding provided by The Science, Technology & Innovation Funding Authority (STDF) in cooperation with The Egyptian Knowledge Bank (EKB). Funding is not applicable to this article (no funds for this research).

Data availability Data sharing is not applicable to this article as no datasets were generated or analyzed during the current study. The availability of data and material is not applicable as there are no data sets used.

Declarations

Competing interests We have no conflict of interest to declare.

Ethical approval Not Applicable (N/A). Fortunately, there are no ethical concerns associated with this work.

References

Abouelez, A.E.: Performance analysis of an *L*-ary PPM MISO ground-to-satellite free-space laser link with an APD-based receiver over a Málaga turbulence channel in the presence of beam wander. J. Opt. Commun. Netw. **14**(3), 100–110 (2022)

Abramowitz, M., Stegun, I.A.: Handbook of Mathematical Functions with Formulas, Graphs, and Mathematical Tables. National Bureau of Standards (1970)

Anbarasi, K., Hemanth, C., Sangeetha, R.G.: A review on channel models in free space optical communication systems. Opt. Laser Technol. **97**, 161–171 (2017)

Andrews, L.C., Phillips, R.L.: Laser beam propagation through random media. Laser Beam Propagation Through Random Media: Second Edition (2005)

Ata, Y., Gökçe, M.C., Baykal, Y.: Mitigation of atmospheric turbulence on up and downlink optical communication systems using receiver diversity and adaptive optics. Opt. Quant. Electron. **54**(10), 1–19 (2022)

Chatzidiamantis, N.D., Karagiannidis, G.K.: On the distribution of the sum of gamma-gamma variates and applications in RF and optical wireless communications. IEEE Trans. Commun. **59**(5), 1298–1308 (2011)

Dharmawansa, P., Rajatheva, N., Ahmed, K.: On the distribution of the sum of Nakagami-*m* random variables. IEEE Trans. Commun. **55**(7), 1407–1416 (2007)

Golbraikh, E., Kopeika, N.S.: Turbulence strength parameter in laboratory and natural optical experiments in non-Kolmogorov cases. Opt. Commun. **242**(4–6), 333–338 (2004)

Gradshteyn, I.S., Ryzhik, I.M.: Table of Integrals, Series, and Products. Academic Press (2014). https://functions.wolfram.com/

Jurado-Navas, A., Garrido-Balsells, J.M., Paris, J.F., Puerta-Notario, A., Awrejcewicz, J.: A unifying statistical model for atmospheric optical scintillation. Numer. Simul. Phys. Eng. Process. **181**(8), 181–205 (2011)

Kiasaleh, K.: Performance of coherent DPSK free-space optical communication systems in K-distributed turbulence. IEEE Trans. Commun. **54**(4), 604–607 (2006)

Kumar, A., Krishnan, P.: Performance analysis of radio-over-free-space optical communication system with spatial diversity over combined channel model. Opt. Quant. Electron. **54**(4), 1–14 (2022)

Li, K., Lin, B., Ma, J.: DPSK modulated multiple apertures receiver system for satellite-to-ground heterodyne optical communication. Opt. Commun. **454**, 124466 (2020)

Liu, X., Lin, M., Kong, H., Ouyang, J., Cheng, J.: Outage performance for optical feeder link in satellite communications with diversity combining. IEEE Wirel. Commun. Lett. **10**(5), 1108–1112 (2021)

Ma, J., Li, K., Tan, L., Yu, S., Cao, Y.: Performance analysis of satellite-to-ground downlink coherent optical communications with spatial diversity over Gamma-Gamma atmospheric turbulence. Appl. Opt. **54**(25), 7575–7585 (2015)
Niu, M., Cheng, J., Holzman, J.F.: Exact error rate analysis of equal gain and selection diversity for coherent free-space optical systems on strong turbulence channels. Opt. Express **18**(13), 13915–13926 (2010)
Niu, M., Cheng, J., Holzman, J.F.: Error rate analysis of M-ary coherent free-space optical communication systems with K-distributed turbulence. IEEE Trans. Commun. **59**(3), 664–668 (2011a)
Niu, M., Schlenker, J., Cheng, J., Holzman, J.F., Schober, R.: Coherent wireless optical communications with predetection and postdetection EGC over gamma–gamma atmospheric turbulence channels. J. Opt. Commun. Netw. **3**(11), 860–869 (2011b)
Osche, G.R.: Optical Detection Theory for Laser Applications. Wiley-Interscience, Hoboken (2002)
Proakis, J.G.: Digital Communications. McGraw-Hill, New York (2001)
Rao, C., Jiang, W., Ling, N.: Spatial and temporal characterization of phase fluctuations in non-Kolmogorov atmospheric turbulence. J. Mod. Opt. **47**(6), 1111–1126 (2000)
Samimi, H., Uysal, M.: Performance of coherent differential phase-shift keying free-space optical communication systems in M-distributed turbulence. J. Opt. Commun. Netw. **5**(7), 704–710 (2013)
Shan, X., Menyuk, C., Chen, J., Ai, Y.: Scintillation index analysis of an optical wave propagating through the moderate-to-strong turbulence in satellite communication links. Opt. Commun. **445**, 255–261 (2019)
Sheng, X., Zhang, Y., Wang, X., Wang, Z., Zhu, Y.: The effects of non-Kolmogorov turbulence on the orbital angular momentum of a photon-beam propagation in a slant channel. Opt. Quant. Electron. **43**(6), 121–127 (2012)
Wang, H., Wang, Q., Wang, Y.: Research on uplink performance of MIMO terrestrial-satellite laser communication based on OSM-MBM joint modulation. J. Mod. Opt. **69**, 1–10 (2022a)
Wang, F., Du, W., Yuan, Q., Liu, D., Feng, S.: Wander of a gaussian-beam wave propagating through Kolmogorov and non-Kolmogorov turbulence along laser-satellite communication uplink. Atmosphere **13**(2), 162 (2022b)
Yasser, M., Ghuniem, A., Hassan, K.M., Ismail, T.: Impact of nonzero boresight and jitter pointing errors on the performance of M-ary ASK/FSO system over Málaga (*M*) M atmospheric turbulence. Opt. Quant. Electron. **53**(1), 1–23 (2021)
Yi, X., Liu, Z.J., Yue, P.: Uplink laser satellite-communication system performance for a Gaussian beam propagating through three-layer altitude spectrum of weak-turbulence. Optik-Int. J. Light Electron Opt. **124**(17), 2916–2919 (2013)
Yue, P., Wu, L., Yi, X., Fu, Z.: Performance analysis of a laser satellite-communication system with a three-layer altitude spectrum over weak-to-strong turbulence. Optik **148**, 283–292 (2017)
Zilberman, A., Golbraikh, E., Kopeika, N.S., Virtser, A., Kupershmidt, I., Shtemler, Y.: Lidar study of aerosol turbulence characteristics in the troposphere: Kolmogorov and non-Kolmogorov turbulence. Atmos. Res. **88**(1), 66–77 (2008a)
Zilberman, A., Golbraikh, E., Kopeika, N.S.: Propagation of electromagnetic waves in Kolmogorov and non-Kolmogorov atmospheric turbulence: three-layer altitude model. Appl. Opt. **47**(34), 6385–6391 (2008b)
Zilberman, A., Golbraikh, E., Kopeika, N.S.: Some limitations on optical communication reliability through Kolmogorov and non-Kolmogorov turbulence. Opt. Commun. **283**(7), 1229–1235 (2010)

Authors and Affiliations

Ahmed Elsayed Abouelez[1]

✉ Ahmed Elsayed Abouelez
a.e.abouelez@eri.sci.eg

[1] Microwave Engineering Department, Electronics Research Institute (ERI), Cairo, Egypt